

SOLID FREEFORM FABRICATION

Comparison of Stainless Steel 316L Parts Made by FDM- and SLM-Based Additive Manufacturing Processes

HAIJUN GONG,^{1,2} DEAN SNELLING,¹ KAMRAN KARDEL,¹
and ANDRES CARRANO¹

1.—Department of Manufacturing Engineering, Georgia Southern University, Statesboro, GA 30460, USA. 2.—e-mail: hgong@georgiasouthern.edu

The selective laser melting (SLM) process is of great interest for fabrication of metal parts, and a number of studies have been conducted to provide in-depth understanding of how stainless steel 316L parts can be fabricated using this powder-bed-fusion-based additive manufacturing (AM) process. In comparison with SLM stainless steel 316L, this paper introduces an innovative AM process for making austenitic stainless steel 316L parts using a metal–polymer composite filament (Ultrafuse 316LX). Stainless steel 316L metal specimens were printed using a material extrusion (FDM)-based three-dimensional (3D) printer loaded with Ultrafuse filament, followed by an industry-standard debinding and sintering process. Tests were performed to understand the material properties, such as hardness, tensile strength, and microstructural characteristics. Part shrinkage was also analyzed based on the features of the FDM stainless steel 316L component. A preliminary guideline on how to select among these two alternative AM processes for fabrication of metal parts is discussed.

INTRODUCTION

Additive manufacturing (AM) or 3D printing has been widely used in the aerospace, biomedical, and robotics industries for manufacture of metal parts.¹ Popular commercialized metal AM technologies include direct metal laser sintering (DMLS), selective laser melting (SLM), laser curing, laser-engineered net shaping (LENS), electron beam melting (EBM), binder jetting (BJ), etc., all of which use metallic powder as raw material.² Ultrasound additive manufacturing (UAM) is a solid-state welding technique based on a hybrid sheet lamination process that combines ultrasonic metal seam welding and computer numerical controlled (CNC) milling. These metal AM technologies are well developed and have been applied in industry and academia for years. At present, AM is not only a methodology for producing complex structures for small-scale production, but also an alternative for advanced manufacturing with high added value. However, all these metal AM processes require large investments for machinery and ancillary facilities to support the high-energy layer-by-layer materials bonding process;³ For example, the SLM

process employs laser energy to melt the metallic powder, demanding inert gas recirculating filtering equipment and a chilling system. Rapid growth of AM or 3D printing will require more economic processes for fabrication of metal parts, and affordable metal AM or 3D printing processes are highly desired for use in small business and university laboratories.

Due to its good corrosion resistance, high strength, and biocompatibility, stainless steel 316L (SS 316L) has been widely used in biomedical applications. Many studies of SLM of SS 316L have been conducted. Kong et al.⁴ and Liverani et al.⁵ investigated the effect of process parameters on the microstructure, biocompatibility, and mechanical and corrosion properties of SLM SS 316L. Sun et al.⁶ improved the scan speed to fabricate high-density SLM SS 316L alloy with low porosity. Bartolomeu et al.⁷ compared the microstructure, mechanical, and wear behavior of austenitic SS 316L produced using three different processing technologies (SLM, hot pressing, and conventional casting). It was found that SLM SS 316L exhibited the best mechanical properties and tribological performance due to its finer microstructure. Ma

et al.⁸ studied the metallurgical behavior of SLM SS 316L and indicated that the cooling rate had a significant effect on the melt pool shape and columnar grain size. The fracture and fatigue properties of SLM SS 316L were also evaluated by Suryawan-shi et al.,⁹ presenting slightly lower values compared with conventionally manufactured SS 316L. Kong et al.¹⁰ also studied heat treatment of SLM SS 316L, indicating that subgrains were widely present in SS 316L alloy while dislocations at the grain boundary migrate and disappear after heat treatment.

However, to date, there have been few studies on materials-extrusion based SS 316L or other metals subjected to AM processing. With the introduction of the newly invented BASF Ultrafuse 316LX metal filament into the AM community, the concept of metal AM will evolve dramatically. The filament is a metal–plastic composite with high loading of metal content. The filament has the same diameter as commonly used plastic filaments and thus fits all open-source fused deposition modeling (FDM)-based 3D printers. The usage of Ultrafuse metal filament is the same as using a plastic filament. The filament is first heated to its glass-transition temperature, then extruded from the nozzle to print a “green” part. Users can customize the parameters and develop new process schemes to achieve a desired density or efficiency. Thereafter, the green part is subjected to a debinding process to remove the plastic content and form a “brown” part, followed by a sintering process to finalize the metal part, as shown in Fig. 1. The debinding and sintering process is the same as the industry-standard process for injection-molded metal parts.¹¹ The objective of this study is to investigate the material properties of a SS 316L part obtained from a green part printed using a low-cost desktop-size 3D printer with Ultrafuse filament, in comparison with SLM SS 316L alloy. The cost efficiency of using Ultrafuse filament for SS 316L parts is evaluated. Preliminary guideline on how to select SLM or FDM for fabrication of metal parts is also discussed.

EXPERIMENTAL METHODS

Ultrafuse 316LX filament with diameter of 1.75 mm was ordered from BASF for this study. The filament is a metal–polymer composite with a nonslip surface, allowing application in any Bowden or direct-drive extruder. A desktop-size Flashforge Dreamer FDM-based 3D printer (Fig. 2) was employed, as used to print plastic filaments such as acrylonitrile butadiene styrene (ABS), poly(lactic acid) (PLA), etc. A set of customized printing parameters (layer thickness, scan speed, extruder temperature, etc.) was developed for this study and used to print green parts. The 3D-printed samples were outsourced to a debinding and sintering service for postprocessing. Catalytic debinding removes the polymer from the part, and sintering in pure hydrogen or vacuum results in the finished metal part. For comparison with SLM, SS 316L parts were also fabricated using SLM-based equipment (Farsoon FS271M). Oerlikon stainless steel gas atomized powder (METCOADD 316L-A) was laser melted to print SS 316L specimens using the machine default process parameters. After fabrication, both the FDM and SLM specimens were

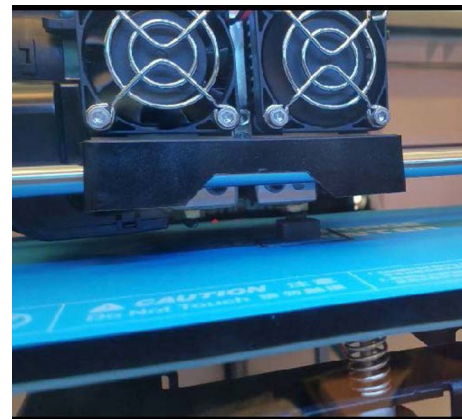


Fig. 2. 3D printing of metal filament green part.

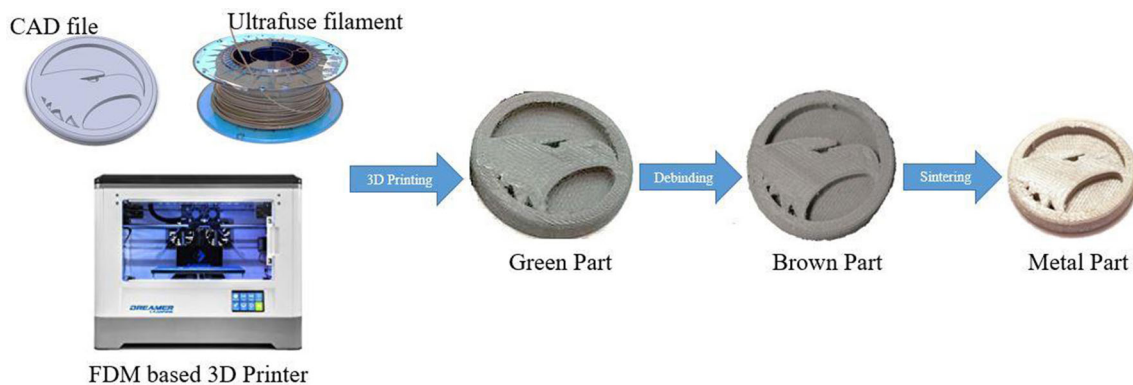


Fig. 1. Schematic of metal 3D printing process using Ultrafuse 316LX filament.

measured using an AccuPyc 1340 gas pycnometer to estimate their density and porosity. The samples were also sectioned, abrasively ground and polished, and etched (with Marble's reagent) for metallography. Their microstructure was examined using an Olympus BX53 M optical microscope. Tensile test specimens (with rectangular cross section) were built horizontally, conforming to ASTM E8. Tensile tests were carried out using an Instron 50-kN tensile testing machine. A Rockwell hardness tester (B scale) was used to measure hardness. An artifact model was designed using SolidWorks with representative geometries to analyze the shrinkage of the FDM SS 316L parts. A Keyence VR-3000 3D measurement system was used for surface measurement of the artifact part.

RESULTS AND DISCUSSION

Density and Porosity

The layer thickness, scan speed, and extruder temperature are critical for melting, extrusion, and deposition of Ultrafuse filament. These parameters were optimized beforehand, in compliance with the criterion of good printing, to yield a consistent thin strand that could be deposited in predetermined locations and adhere to the solidified prior layer. As voids are coherently included in the printed part, the FDM process cannot build fully dense samples. It was found that layer thickness of 0.2 mm, scan speed of 60 mm/s, and extruder temperature of 235°C were appropriate parameter values to print the desired part, with consistent surface topography and laminations. The other parameters were set to the factory defaults of the 3D printer. The green parts were debound and sintered to form the SS 316L metal part. The density was measured to be 7.88 g/cm³, comparable to SLM SS 316L material (8 g/cm³) and AISI type 316L stainless steel (8 g/cm³). Hence, it can be said that the porosity of the

FDM SS 316L was around 1.5%, while the SLM SS316L part was relatively fully dense and without apparent porosity.

Microstructure

The microstructure of the FDM and SLM SS 316L alloy is shown in Fig. 3. After debinding the plastic component from the green part, sintering was carried out in a furnace to densify the metal component of the brown part. Within a pure hydrogen atmosphere or vacuum, small grains are recrystallized and grow to form a set of strain-free equiaxed grains. As shown in Fig. 3a, the austenitic SS 316L alloy exhibited grains with approximately equal dimensions in all directions. The grain size depends on both the duration and temperature of sintering. The grains are characteristic of the annealed condition without apparent dislocations. The SLM SS 316L (Fig. 3b) showed full gamma austenite phase containing subgrains, and the grain size for the SLM 316L increased with increasing laser power. Abundant subgrain boundaries with high density of dislocations accounted for its good plasticity.⁴ It can be predicted that the FDM SS 316L sample will exhibit higher ductility compared with SLM samples. Otherwise, the FDM SS 316L grains are independent of the build direction. There is no layer effect along the build direction. All grains were uniformly arranged, indicating isotropic mechanical properties. The microstructure of SLM SS 316L clearly showed the melt pools of each laser melting track. The orientation of the melt pool implies that the material properties of the SLM SS 316L will be anisotropic.

Tensile Strength and Hardness

FDM SS 316L tensile specimens were directly printed then postprocessed to obtain the metal part. The specimens shrank after the sintering process.

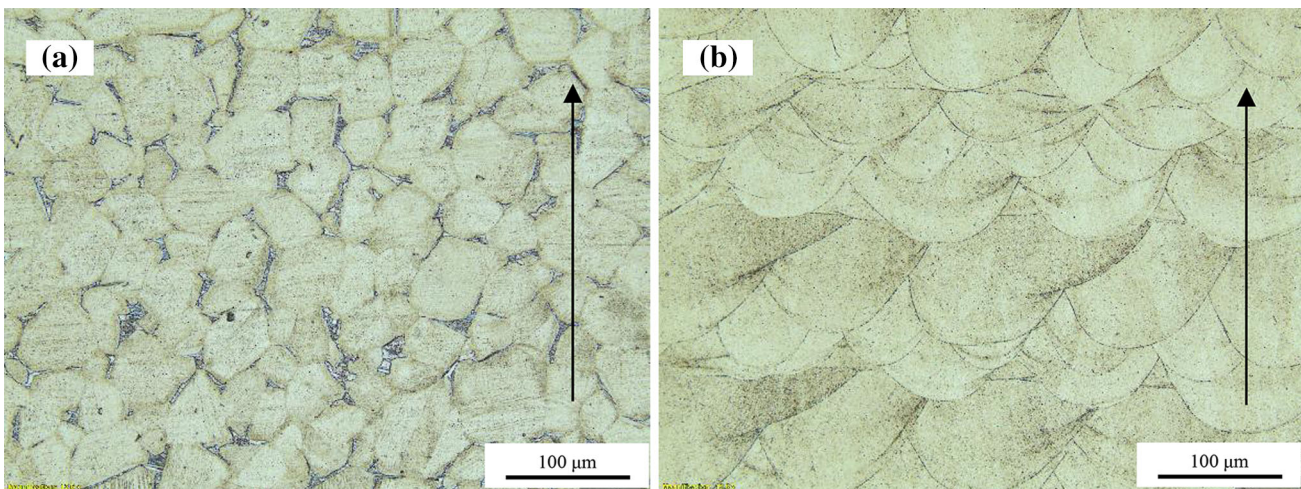


Fig. 3. Optical microscopy of Ultrafuse SS 316L microstructure (after sintering) and SLM SS 316L microstructure (arrow indicates build direction)

Table I. Tensile properties of SS 316L alloy

	<u>FDM SS 316L</u>	<u>SLM SS 316L</u>	<u>AISI type SS 316L^a</u>
Yield strength (MPa)	167	541	205
UTS (MPa)	465	648	515
Elongation at break (%)	31	30	60
Young's modulus (GPa)	152	320	193

^a<http://asm.matweb.com/search/SpecificMaterial.asp?bassnum=mq316q>.

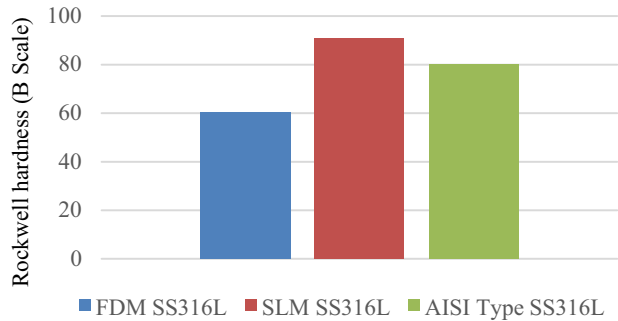


Fig. 4. Rockwell hardness (B scale) testing result of SS 316L.

The tensile properties of the FDM and SLM SS 316L, such as yield strength, ultimate tensile strength (UTS), elongation at break, and elastic modulus, are presented in Table I, in comparison with those of AISI type SS 316L. The results of these tests indicate that FDM SS 316L alloy has lower yield strength, UTS, and elastic modulus, which can be attributed to its equiaxed grains and austenitic microstructure. The major tensile properties are even lower than those of AISI type SS 316L (annealed material). The inherent porosity inclusion may deteriorate the ductility of the material due to local stress concentrations, so that the elongation of FDM SS 316L was much lower than that of AISI type SS 316L (31% versus 60%). Because of the abundant subgrain boundaries with high dislocation density, dislocations start blocking the motion of each one. Therefore, SLM SS 316L exhibited higher yield strength, UTS, and Young's modulus, and accordingly lower ductility. However, the SLM SS 316L is less influenced by porosity, considering its as-built material density. The Rockwell hardness (B scale) testing result is shown in Fig. 4. It can be seen that the hardness value of FDM SS 316L is also lower than that of SLM or AISI type SS 316L. The SLM SS 316L showed slightly higher hardness than AISI type SS 316L, in agreement with the microstructural analysis and discussion of the tensile properties above.

Shrinkage

Various studies have been carried out on accuracy analysis and error compensation for SLM metal

parts. A thermal model and experiments are usually coupled to compensate the geometrical variation of SLM parts.^{12,13} Therefore, this section only concentrates on the shrinkage of the FDM SS 316L metal part. Shrinkage analysis was performed on an artifact part printed using Ultrafuse filament, as shown in Fig. 5. A set of features of interest (FOIs) were marked on the computer-aided design (CAD) model with a sequence number. The dimension of each FOI on the green part and metal part was measured to compare the size variation and determine the shrinkage rate. The green part was measured using the Keyence VR-3000 at the FOIs before being sent for debinding and sintering. The metal (sintered) part (Fig. 5c) was also measured using the same equipment to compare with the FOIs of the green part and thus estimate the shrinkage.

As shown in Fig. 5c, the metal part apparently shrank after the sintering process. The metal part had similar shape characteristics but decreased size due to the shrinkage. However, the major FOIs retained the features of the geometrical configuration, ensuring that the FDM-based metal AM can form metal parts using Ultrafuse filament, as long as the shrinkage is compensated when printing the green part. The size of the FOIs in the x - y plane (diameter and edge length) and along the z -axis (height and depth) are of great interest in this study. The percentage of FOI shrinkage is presented in Table II. Note that the feature shrinkage in the x - y plane was slightly influenced by their z -axis level. A feature at a lower level may thus shrink less than the same feature at a higher level. Also, greater height or depth variation tends to occur at lower levels along the z -axis. Overall, the calculated percentage shrinkage rate along the z -axis was higher than for the geometrical features in the x - y plane, which can be attributed to the effect of gravity on the metal component during the sintering process.

In addition, a couple of side holes were designed with multiple geometries to verify that unsupported features could be printed. Figure 5b shows the green part of the artifact which was directly printed using Ultrafuse filament. Note that all the unsupported features were printed without apparent distortion. This demonstrates that the extruded

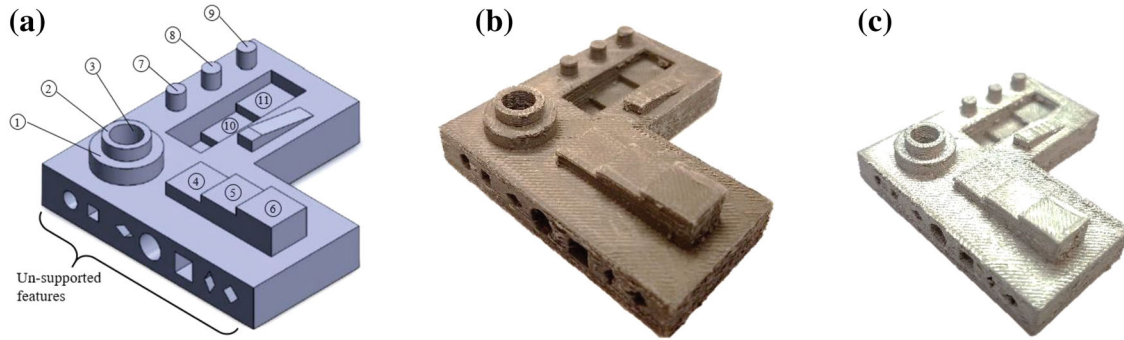


Fig. 5. Shrinkage analysis of artifact part, (a) CAD file, (b) green part, and (c) metal part.

Table II. Shrinkage of artifact part

FOI	Shrinkage	
	$x-y$	z
#1	14%	23%
#2	18%	20%
#3	18%	—
#4	13%	22%
#5	16%	22%
#6	17%	19%
#7	13%	23%
#8	13%	23%
#9	13%	23%
#10	—	18%
#11	—	15%

filament exhibits great shape retention due to its fast phase transformation from viscous to solid state.

Preliminary Guideline for Selecting the FDM- or SLM-Based Metal AM Process

It has been demonstrated that the SLM-based metal AM process can produce complex structures and geometrical features directly from a variety of metallic powders. Industries and research institutions are increasingly getting involved in SLM or similar technologies. However, there are many benefits of using Ultrafuse filament for 3D printing of metal parts, compared with other metal AM processes. Firstly, the investment in terms of machinery and ancillary facilities is low. An FDM-based 3D printer is much less expensive than an SLM-based metal AM machine and can be easily operated and maintained by users. Secondly, the metal filament is affordable and easier to handle than metallic powders; For instance, a couple of kilograms of metallic powder must usually be loaded into a SLM machine to start a build, with unmelted powder being sieved and recycled for the next build. Safety protection and precautions are always needed when handling metallic powders, especially reactive ones (titanium, aluminum, etc.).

In contrast, only the required quantity of metal filament need be used, and this can be predicted. Thirdly, the FDM-based 3D printer is immediately ready to accept the next build when the green part is completed and removed. Also, the metal filament can be used for printing in an open chamber at room temperature, in contrast to the SLM process (which requires a chamber filled with inert gas) or the EBM process (which requires a vacuum chamber). This greatly reduces the lead time required for machine cleaning, material recycling, and chamber preparation, representing a substantial cost advantage for production of metal AM parts. Therefore, the FDM-based metal AM process is suitable for use in small business and university laboratories with limited budgets and lower accuracy requirements, in contrast to SLM-based metal AM technologies.

CONCLUSION

This study compares fabrication of metal AM parts using FDM- and SLM-based approaches. Ultrafuse 316LX filament was introduced for metal 3D printing. The FDM-based process is easier to handle and less expensive than SLM-based metal AM technologies. The microstructure of the austenitic FDM SS 316L alloy consisted of strain-free equiaxed grains. The tensile strength and hardness of FDM and SLM SS 316L specimens were examined and compared with those of ANSI type SS 316L. The shrinkage of the FDM SS 316L from the green to metal part varied in the $x-y$ plane and along the z -axis. However, use of Ultrafuse filament for 3D printing is a cost-effective approach for making metal AM parts when the accuracy requirements are not as rigorous as for the SLM process.

ACKNOWLEDGEMENT

The authors acknowledge Dr. Shanshan Zhang and the staff of the Rapid Prototyping Center at the University of Louisville for help with material property testing.

REFERENCES

1. J.J. Lewandowski and M. Seifi, *Annu. Rev. Mater. Res.* 46, 151 (2016).

2. I. Gibson, D.W. Rosen, and B. Stucker, *Additive Manufacturing Technologies: Rapid Prototyping to Direct Digital Manufacturing* (Berlin: Springer, 2009).
3. D.S. Thomas and S.W. Gilbert, *NIST Spec. Publ.* (2014). <https://doi.org/10.6028/NIST.SP.1176>.
4. D. Kong, X. Ni, C. Dong, X. Lei, L. Zhang, C. Man, J. Yao, X. Cheng, and X. Li, *Mater. Des.* 152, 88 (2018).
5. E. Liverani, S. Toschi, L. Ceschini, and A. Fortunato, *J. Mater. Process. Technol.* 249, 255 (2017).
6. Z. Sun, X. Tan, S.B. Tor, and W.Y. Yeong, *Mater. Des.* 104, 197 (2016).
7. F. Bartolomeu, M. Buciumeanu, E. Pinto, N. Alves, O. Carvalho, F.S. Silva, and G. Miranda, *Addit. Manuf.* 16, 81 (2017).
8. M. Ma, Z. Wang, and X. Zeng, *Mater. Sci. Eng. A* 685, 265 (2017).
9. J. Suryawanshi, K.G. Prashanth, and U. Ramamurty, *Mater. Sci. Eng. A* 696, 113 (2017).
10. D. Kong, X. Ni, C. Dong, L. Zhang, C. Man, J. Yao, K. Xiao, and X. Li, *Electrochim. Acta* 276, 293 (2018).
11. A. Páez-Pavón, A. Jiménez-Morales, T.G. Santos, L. Quintino, and J.M. Torralba, *J. Magn. Magn. Mater.* 416, 342 (2016).
12. S. Afazov, W. Denmark, B.L. Toralles, A. Holloway, and A. Yaghi, *Addit. Manuf.* 17, 15 (2017).
13. Y. Liu, Y. Yang, and D. Wang, *Int. J. Adv. Manuf. Technol.* 90, 2913 (2017).